ACS NANO Caltech Library

Subscriber access provided by Caltech Library

Article

Atomic H-Induced MoC Hybrid as an Active and Stable Bifunctional Electrocatalyst

Xiujun Fan, Yuanyue Liu, Zhiwei Peng, Zhenhua Zhang, Haiqing Zhou, Xianming Zhang, Boris I. Yakobson, William A. Goddard, Xia Guo, Robert H. Hauge, and James M. Tour

ACS Nano, **Just Accepted Manuscript** • DOI: 10.1021/acsnano.6b06089 • Publication Date (Web): 18 Dec 2016

Downloaded from http://pubs.acs.org on December 19, 2016

Just Accepted

"Just Accepted" manuscripts have been peer-reviewed and accepted for publication. They are posted online prior to technical editing, formatting for publication and author proofing. The American Chemical Society provides "Just Accepted" as a free service to the research community to expedite the dissemination of scientific material as soon as possible after acceptance. "Just Accepted" manuscripts appear in full in PDF format accompanied by an HTML abstract. "Just Accepted" manuscripts have been fully peer reviewed, but should not be considered the official version of record. They are accessible to all readers and citable by the Digital Object Identifier (DOI®). "Just Accepted" is an optional service offered to authors. Therefore, the "Just Accepted" Web site may not include all articles that will be published in the journal. After a manuscript is technically edited and formatted, it will be removed from the "Just Accepted" Web site and published as an ASAP article. Note that technical editing may introduce minor changes to the manuscript text and/or graphics which could affect content, and all legal disclaimers and ethical guidelines that apply to the journal pertain. ACS cannot be held responsible for errors or consequences arising from the use of information contained in these "Just Accepted" manuscripts.

ACS Publications

ACS Nano is published by the American Chemical Society. 1155 Sixteenth Street N.W., Washington, DC 20036

Published by American Chemical Society. Copyright © American Chemical Society. However, no copyright claim is made to original U.S. Government works, or works produced by employees of any Commonwealth realm Crown government in the course of their duties.

Atomic H-Induced Mo_2C Hybrid as an Active and Stable Bifunctional Electrocatalyst

Xiujun Fan,[†‡⊥∥] * *Yuanyue Liu,[¶ς]* *Zhiwei Peng,[⊥]* *Zhenhua Zhang,[#]* *Haiqing Zhou,[⊥∥]* *Xianming Zhang,[†]* *Boris I. Yakobson,[⊥∥§]* *William A. Goddard III,[¶]* *Xia Guo,[‡]** *Robert H. Hauge[⊥∥1]* *and James M. Tour[⊥∥§]**

[†]Institute of Crystalline Materials, Shanxi University, Taiyuan, Shanxi 030006, China

[‡]College of Electronic Information and Control Engineering, [#]Institute of Microstructures and Properties of Advanced Materials, Beijing University of Technology, Beijing 100124, China

[⊥]Department of Chemistry, [∥]NanoCarbon Center, [§]Department of Materials Science and NanoEngineering, Rice University, Houston, Texas 77005, United States

[¶]Materials and Process Simulation Center, [ς]The Resnick Sustainability Institute, California Institute of Technology, Pasadena, CA 91125, United States

E-mail: tour@rice.edu, guo@bjut.edu.cn, fxiujun@gmail.com

Abstract Mo_2C nanocrystals (NCs) anchored on vertically aligned graphene nanoribbons (VA-GNR) as hybrid nanoelectrocatalysts (Mo_2C-GNR) are synthesized through the direct carbonization of metallic Mo with atomic H treatment. The growth mechanism of Mo_2C NCs with atomic H treatment is discussed. The Mo_2C-GNR hybrid exhibits highly active and durable electrocatalytic performance for the hydrogen evolution reaction (HER) and oxygen reduction reaction (ORR). For HER, in an acidic solution the Mo_2C-GNR has an onset potential

[1] Deceased March 17, 2016

of 39 mV and a Tafel slope of 65 mV dec^{-1}, in a basic solution Mo_2C-GNR has an onset potential of 53 mV, and Tafel slope of 54 mV dec^{-1}. It is stable in both acidic and basic media. Mo_2C-GNR is a high activity ORR catalyst with a high peak current density of 2.01 mA cm^{-2}, an onset potential of 0.93 V that is more positive *vs* reversible hydrogen electrode (RHE), a high electron transfer number *n* (~3.90) and long-term stability.

Keywords: Mo_2C, graphene nanoribbon, hydrogen evolution reaction (HER), oxygen reduction reaction (ORR), atomic H

The electrocatalytic hydrogen evolution reaction (HER) and oxygen reduction reaction (ORR) hold tremendous promise as efficient and clean energy solutions. Although platinum-group metals (PGMs) Pt,[1] Rh,[2] and Pd,[3] are highly active and stable electrocatalysts for HER and ORR, their scarcity and high cost hinder their large-scale commercial applications. Hence, some earth-abundant transition metal carbides (TMCs), such as WC[4] and particularly Mo_2C[5] have emerged and they exhibit remarkable HER and ORR performances due to their electronic structures that are similar to those of noble metals.[6] Mo_2C-based materials with various nanostructures have been designed to be HER catalysts, including nanotubes,[7] nanowires,[8] and nanoparticles.[9] Recent studies have shown that composites consisting of Mo_2C and carbon are active toward hydrogen evolution in acidic electrolytes, such as Mo_2C/carbon xerogel (CXG),[10] Mo_xC-Ni@N-doped carbon vesicle,[11] Mo_2C–graphene,[12] Mo_2C/reduced

graphene oxide,[13] MoO_2/Mo_2C-N-doped carbon nanotubes (NCNTs),[14] Mo_2C@nitrogen-rich carbon,[15] and Mo_2C/graphitic carbon sheets.[16] Nonetheless, the key issue for the development of carbide catalysts is their synthesis, especially catalysts with nanocrystalline phases, because of the expected aggregation and/or disproportionate growth of Mo_2C nanocrystals (NCs) at elevated reaction temperatures, and the swift oxidation of Mo_2C nanoparticles (NPs) surfaces to MoO_x species on exposure to air.[17]

The usual process to synthesize metal carbides involves high temperature (> 1000 °C) carburization of metals with graphitic carbon, which is not suitable to producing materials for catalytic applications because the products have low surface areas.[18] The temperature-programmed reduction (TPR) method was developed in the 1980s and extensively used to synthesize high surface area transition-metal nitrides and carbides.[19] Nevertheless, the TPR conditions are demanding. More recently, gas-phase reactions of volatile metal compounds,[5] pyrolysis of metal complexes[20] and solution reactions[21] were used to synthesize metal carbides using costly or toxic reagents such as MoF_6[22] or $Mo(CO)_6$.[23] Unfortunately, chars from the pyrolysis of the carbon usually contaminate the resultant carbide.[24] Coincidentally, quite recently, functionalized 2D layered metal carbides/carbonitrides (MXene) including Mo_2C have been synthesized by selective etching with concentrated HF or a solution of LiF and HCl. Such chemically derived Mo_2C suffers from severe structural defects, is terminated by hydroxyl and/or other oxygen-containing groups, and has fluorine present on the surface.[25] Furthermore, hot-filament chemical vapor deposition (HF-CVD) is one of the most promising techniques for

growing high melt point carbide materials at relatively low substrate temperature, such as WC,[26] M_3C (M:Fe,Co,Ni),[27] silicon carbide (SiC)[28] and so on. In the HF-CVD processing, the filament was heated to over 2000 ^oC for activation of the source gas. It is highly flexible and scalable, easy to scale up to large-scale growth and, no less important, utilizes metal rather than vaporized metal-containing reagents as precursors, which introduce no other impurity. From the applications point of view, although Mo_2C-based materials have been extensively studied for HER in acidic media, it is still challenging to develop Mo_2C-based HER catalysts that work efficiently over a range of pH values. Moreover, Mo_2C materials draw much less attention in ORR.[29] Only recently have these carbides been shown to be efficient noble metal-free catalysts for ORR.[30] The dual use of the Mo_2C-based materials for both HER and ORR applications is a challenging issue that has been scarcely reported.

Herein, we report a synthesis of a highly active and stable precious-metal-free hybrid electrocatalyst consisting of Mo_2C NCs anchored on vertically aligned graphene nanoribbon (VA-GNR)**.** The VA-GNR supported-Mo_2C (Mo_2C-GNR) hybrid is prepared with atomic H treatment through the direct reaction of metallic Mo with a carbon source. The Mo_2C-GNR hybrid demonstrates excellent HER performance both in acidic and alkaline electrolytes, with the overpotential for driving a current of 10 mA cm^{-2} (η_{10}) of 152 mV, onset potential of 39 mV and Tafel slop of 65 mV dec^{-1} in acid solution, and 121 mV, 53 mV and 54 mV dec^{-1}, respectively, in alkaline media. The Mo_2C-GNR is also a highly active catalyst for ORR with a high peak current density of 2.01 mA cm^{-2}, a more positive onset potential of 0.93 V *vs* reversible hydrogen

electrode (RHE) and a high electron transfer number *n* (~3.90). The dual performance of Mo_2C-GNR in both HER and ORR suggests a material type as nonprecious metal bifunctional catalysts.

Results and Discussion

The experimental setup for the preparation of Mo_2C-GNR is depicted in Figure 1a. First, VA-GNR was made from vertically aligned carbon nanotubes (VA-CNTs) through a hot filament chemical vapor deposition (HF-CVD) process.[31] After a thin layer of Mo (~75 nm) was deposited atop the VA-GNR, the prepared structure was subjected to atomic H treatment for carburization of metallic Mo. Mo_2C without VA-GNR support was prepared at the same time for comparison. Scanning electron microscopy (SEM) was carried out to study the morphology of VA-GNR before and after atomic H treatment (Figure 1b-e). As shown in Figure 1b and Figure S1-S2, the unzipped VA-GNR have clumps of tips that meet together, forming structures resembling Native American "teepees".[32] The teepees are distributed with enough open space to permit the Mo particles to pass through the VA-GNR bundles and disperse on the surface of the VA-GNR. Based on imaging, there is limited agglomeration of the Mo, which appears as a film to the eye (Supporting Information, Figure S3). With atomic H treatment, Mo_2C NCs form along the surface of the VA-GNR, which maintains the vertical structural integrity and alignment (Figure 1c and S4). The SEM top view image shows that the Mo_2C grains are uniformly dispersed without visible aggregation (Figure 1d), and not stacked on the tips of VA-GNR, which

is different from previous studies about iron group metal carbide NCs prepared with same the method.[27] This means that the properties of the elements themselves such as the melting points and vapor pressures may play a role in NCs growth with HF-CVD process. The cross-sectional image reveals the porous structure of the VA-GNR forest, while Mo_2C grains are difficult to distinguish due to their small size (Figure 1e). As a control, Mo_2C synthesized directly on Si without the GNR support produced larger particles, as shown in the SEM image (Supporting Information, Figure S5). This control experiment demonstrates the important role of VA-GNR in the formation of Mo_2C NCs with uniform dispersion and small particle size, which are critical for the high electrocatalytic activities.

Raman spectra (Figure 1f and S6a) and powder X-ray diffraction (XRD) patterns (Figure 1g and S6b) acquired from VA-GNR, Mo@VA-GNR and Mo_2C-GNR are performed to studied the physical and chemical structures evolution of these carbon hybrid. From the Raman spectrum and XRD pattern of Mo@VA-GNR in Figure S6, it is confirmed that Mo layer deposited on VA-GNR was partly converted to MoO_3 when the sample is exposed to air.[33] With atomic H treated for 6 h, the Mo_2C-GNR reveals peaks at 1592 cm^{-1} (G-band) and 2676 cm^{-1} (2D-band), followed by a shoulder peak at 2927 cm^{-1} (D+G) (Figure 1f). The area ratios of G-band to D-band (I_G/I_D) are 1.34 and 1.27 for VA-GNR and Mo_2C-GNR, respectively, indicating that litter disorder is introduced by atomic H treatment.[16] There are no noticeable peaks in the low range from 100 to 1200 cm^{-1} for Mo_2C-GNR (dashed circle in Figure 1f), indicating that the sputtered Mo and the relevant MoO_3 have been transformed into Mo_2C with atomic H treatment. In

Figure 1g, the diffraction peaks at 34.6°, 38.1°, 39.6° and 52.4° can be assigned to the (100), (002), (101) and (102) crystal faces of Mo_2C with a hexagonal closed-packed structure (PDF#35-0787). The carbon peak of (101) is from the GNR support, which corresponds to the XRD result of VA-GNR. No any peaks from metallic Mo or MoO_3 are detected, indicative of a successful chemical conversion of Mo into Mo_2C.

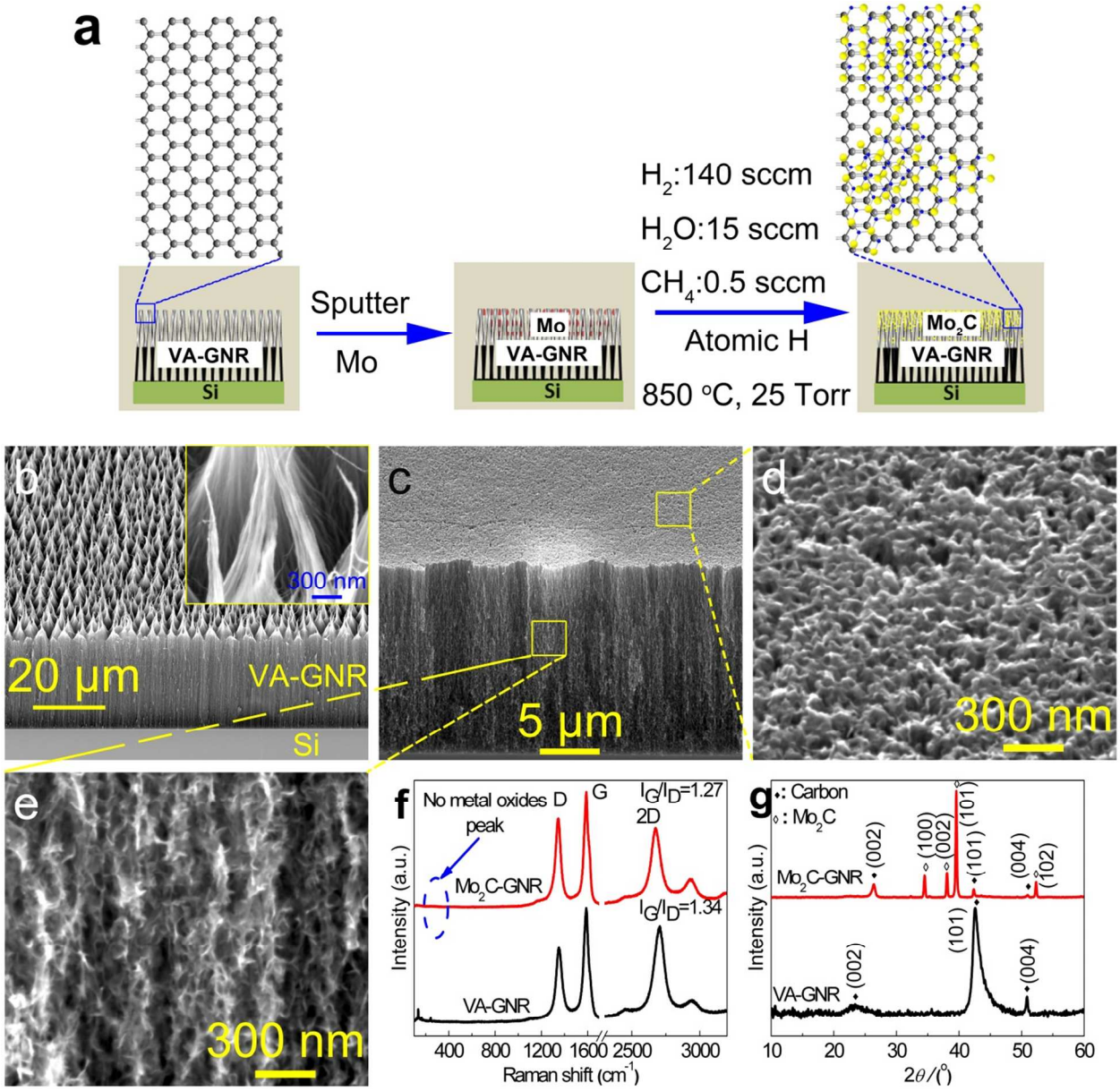

Figure 1. (a) The scheme depicting the key process for Mo_2C NC growth, in which a layer of Mo is deposited on VA-GNR using a sputter system. SEM images of (b) VA-GNR, (c-e) Mo_2C-GNR hybrid. (f) Raman spectra and (g) XRD patterns of pristine VA-GNR and Mo_2C-GNR hybrid.

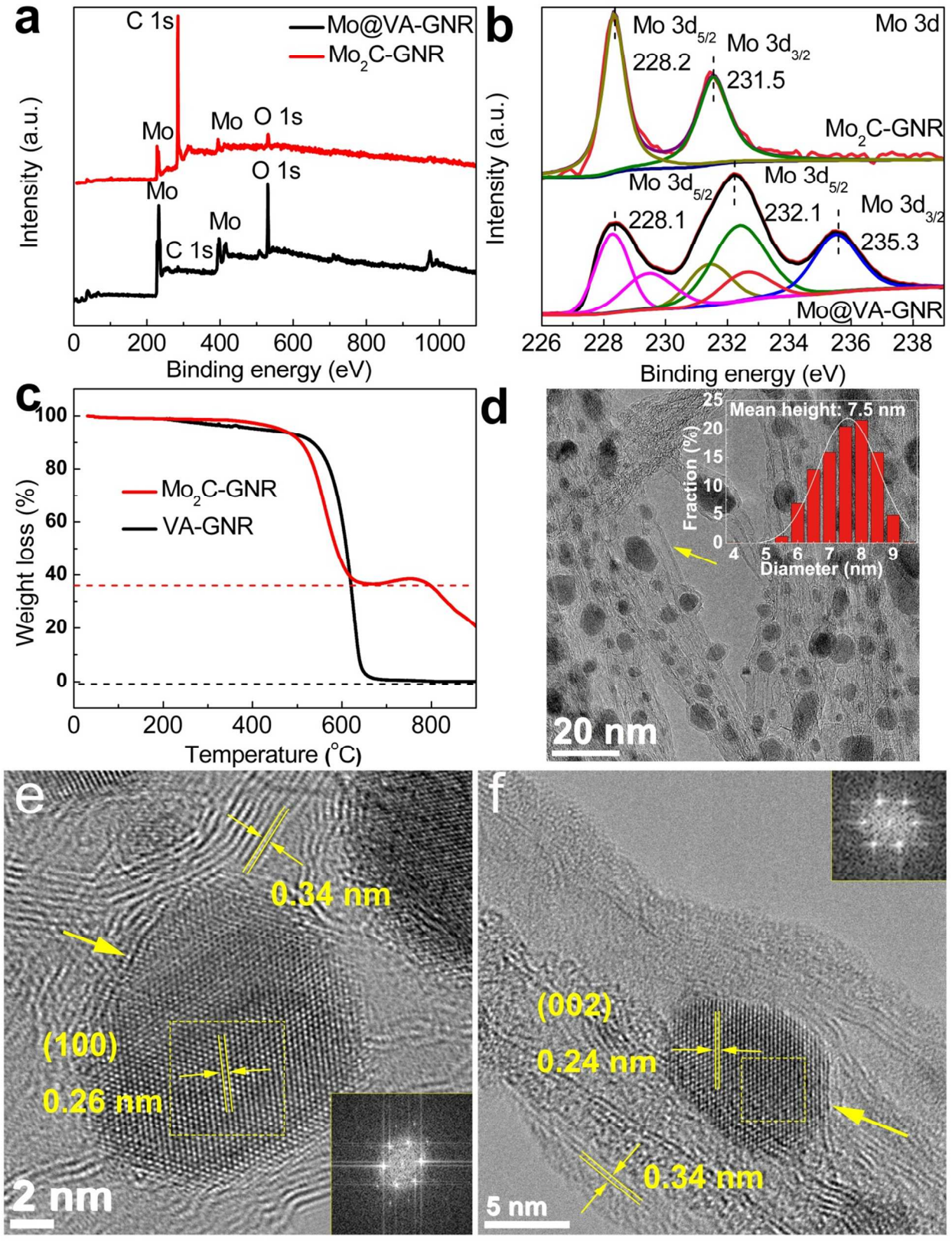
a
C 1s
Mo@VA-GNR
Mo2C-GNR
Mo
Mo
O 1s
O 1s
Mo
Mo
C 1s
Intensity (a.u.)
0
200
400
600
800
1000
Binding energy (eV)
b
Mo 3d5/2
228.2
Mo 3d3/2
231.5
Mo 3d
Mo2C-GNR
Mo 3d5/2
228.1
Mo 3d5/2
232.1
Mo 3d3/2
235.3
Mo@VA-GNR
Intensity (a.u.)
226
228
230
232
234
236
238
Binding energy (eV)
c
Mo2C-GNR
VA-GNR
Weight loss (%)
100
80
60
40
20
0
0
200
400
600
800
Temperature (°C)
d
Mean height: 7.5 nm
Fraction (%)
25
20
15
10
5
0
4
5
6
7
8
9
Diameter (nm)
20 nm
e
0.34 nm
(100)
0.26 nm
2 nm
f
(002)
0.24 nm
0.34 nm
5 nm

Figure 2. (a) XPS survey spectrum and (b) high resolution XPS scan of the Mo 3d of Mo@VA-GNR and Mo_2C-GNR. (c) TGA curves of the VA-GNR and Mo_2C-GNR hybrid measured by heating samples in air flow to 900 °C at a ramp of 5 °C min^{-1}. (d) TEM image of Mo_2C-GNR prepared at 850 °C for 6 h. Inset: Gaussian fits of the size distribution of Mo_2C NCs. (e, f) HR-TEM images of individual Mo_2C NCs with (100) plane and (002) plane. Thin layers of carbon species (indicated by yellow arrows) are observed. The insets in (e, f) show the corresponding fast Fourier transform (FFT) patterns of the flat surface enclosed by the yellow boxes on each image.

Further investigation of the composition and crystalline structure of the Mo_2C-GNR hybrid was performed by X-ray photoelectron spectroscopy (XPS, Figure 2a,b), thermal gravimetric analysis (TGA, Figure 2c) and transmission electron microscope (TEM, Figure 2d-f). From Figure 2a, elements of C, O and Mo can be clearly identified. The main C1s peaks at 284.5 eV are observed for both Mo@VA-GNR and Mo_2C-GNR (Supporting Information, Figure S7a), which is consistent with the sp^2 carbon of the GNR scaffold. For Mo@VA-GNR, the peak at 228.1 eV is attributed to metallic Mo, while the peaks at 232.1 and 235.3 eV are are indexed with MoO_3, which results from surface oxidation of the Mo when the sample is exposed to air. For Mo_2C-GNR, the peaks located at binding energies of 228.2 eV and 231.5 eV are assigned to Mo^{2+} ($3d_{5/2}$ and $3d_{3/2}$, respectively), which is consistent with the carbide phase (Figure 2b). The O 1s peak at 530.4 eV is correspond to the lattice O_2^- in the MoO_3 (Supporting Information,

Figure S7b). While, with atomic H treatment, the O 1s peak is obviously shifted from 530.4 eV to 532.8 eV, which is attributed to absorbed oxygen on the surface of Mo_2C-GNR. This result is also consistent with the Mo 3d XPS spectra of Mo_2C-GNR in Figure 2b. The elemental composition determined by the inductively coupled plasma mass spectrometry (ICP-MS) and the surface atomic concentrations derived by energy-dispersion X-ray spectroscopy (EDS, Figure S8) are summarized in Table S1. Mo@VA-GNR and Mo_2C-GNR have an almost constant Mo content of ~ 31 wt%. Mo@VA-GNR has an O content of 50.6 at% derived from the EDS measurements. In contrast, after atomic H treatment the O content decreases significantly to 3.5 at%, which may be due to the reduction of MoO_3 and carbonization of Mo at VA-GNR in atomic H at 850 °C.[34]

Confirmed by TGA, no significant weight loss is detected below 500 °C in air for Mo_2C-GNR (Figure 2c). When the temperature rises above 500 °C, the decrease in weight starts and continues until 645 °C, and displays a mass increase, followed by a mass decrease, which confirms the formation of MoO_3 solid residue.[34] Furthermore, all of the TEM observed Mo_2C is inlaid or anchored on the GNR; few of any free-standing particles were found away from the GNR support (Figure 2d). Some nanotube-like carbon remains from unopened CNTs (yellow arrow). A few layers of graphite shell surround these irregularly shaped granular particles, as shown in Figure 2d. The shell structure is likely formed during the cooling of the HF-CVD system due to the active carbon dissolution-precipitation process for transition metals.[35] Covalent bonding between the graphite shells and Mo_2C could further downshift the d-band center of

molybdenum, and thereby decrease its hydrogen binding energy.[24] A Gaussian fit gives a most common diameter of 7.5 nm (inset in Figure 2d). In contrast, the Mo_2C on Si without GNR support forms larger aggregates, as shown in the TEM image (Supporting Information, Figure S9). Therefore, it can be concluded that the VA-GNR effectively prevented the aggregation and growth of the reduced Mo_2C NCs. The high-resolution TEM (HR-TEM) images allow us to observe the crystalline nature of the Mo_2C NCs produced. Figures 2e,f exhibite that the lattice fringes with a d-spacing of 0.26 and 0.24 nm, closely match the (100) and (002) planes of hexagonal Mo_2C, respectively, and are also consistent with the XRD result (Figure 1f). The size of the Mo_2C NCs are vary with different atomic H treatment time. With atomic H treatment for 3 h, the Mo_2C NCs ranged from 3 to 5 nm and decorated the carbon layer without obvious aggregation (Figure S10a,b). Upon increasing the treatment time to 9 h, the Mo_2C NCs exhibit larger nanoparticles (Figure S10c,d). The larger size could be due to the migration and ripening of the NCs during the reduction. The continuous lattice fringes throughout the entire nanoparticle shown in the HR-TEM image (Figure S10) together with the sharp peaks in the XRD patterns (Figure S11) imply the efficiency of the atomic H treatment to produce high crystallinity and pure phase Mo_2C NCs.[36] High-angle angular dark-field scanning transmission electron microscopy (HAADF-STEM) and the corresponding elemental mappings (EDS) reveal the uniform distribution of C and O elements over the Mo_2C-GNR prepared with atomic H treatment for 9 h (Figure S12). Mo element is covered on the interior of the C and O elements, also suggesting that the Mo_2C NCs are mainly attached over the carbon support to form a hybrid.

In the TPR reaction, the mechanism for the MoO_3 to Mo_2C conversion involves the substitution of carbon for oxygen in the MoO_3 lattice, with little displacement of the Mo atoms.[22] However, in the HF-CVD process, the temperature of the system is far above the temperature regime where MoO_3 is unstable with respect to decomposition into MoO_2 followed by the MoO_2 itself decomposing to give Mo metal.[37] Therefore, The growth of Mo_2C NCs is through the direct carburization of Mo metal, without forming any reaction intermediate such as MoO_2. That is, MoO_3 is reduced to metallic Mo mainly by atomic H, followed by simultaneous C insertion at high temperature. The addition of the hot filament step in the synthetic route is critical to the formation of Mo_2C NCs. It not only assists to form active carbon that diffuses into the Mo surface and reacts with Mo, but also creates excessive atomic H that activates the Mo surface *via* reduction of MoO_3 and catalyzes the crystallization of Mo_2C. Eq 1-4 outline the mechanism of the Mo_2C formation with atomic H treatment. The activated gas mixtures of atomic H (H*, eq 1) and carbon-containing species (eq 2), are generated under high temperature of the filament (> 2000 °C) in the HF-CVD system. MoO_3 is reduced by H* to metallic Mo in eq 3.[38] The generated C* is so active that it reacts directly with metallic Mo to form Mo_2C NCs at the high temperature in eq 4.

$$H_2 \rightarrow H^* \ (1)$$
$$CH_4 \rightarrow C^* + H^* \ (2)$$
$$\mathrm{MoO_3} + H^* \rightarrow \mathrm{Mo} + H_2O \ (3)$$
$$Mo + C^* \xrightarrow{H^*} Mo_2C \ (4)$$

The specific surface area of the pristine VA-GNR and Mo_2C-GNR measured by N_2 adsorption using Brunauer-Emmett-Teller (BET) measurements (see Supporting Information,

Figure S13) are 936.4 and 641.1 $m^2 g^{-1}$, respectively. The decrease of the specific surface area of Mo_2C-GNR can be attributed to the decoration of Mo_2C NCs on the surface of VA-GNR. This high surface area can provide sufficient space for electrocatalytic performance of HER and ORR.

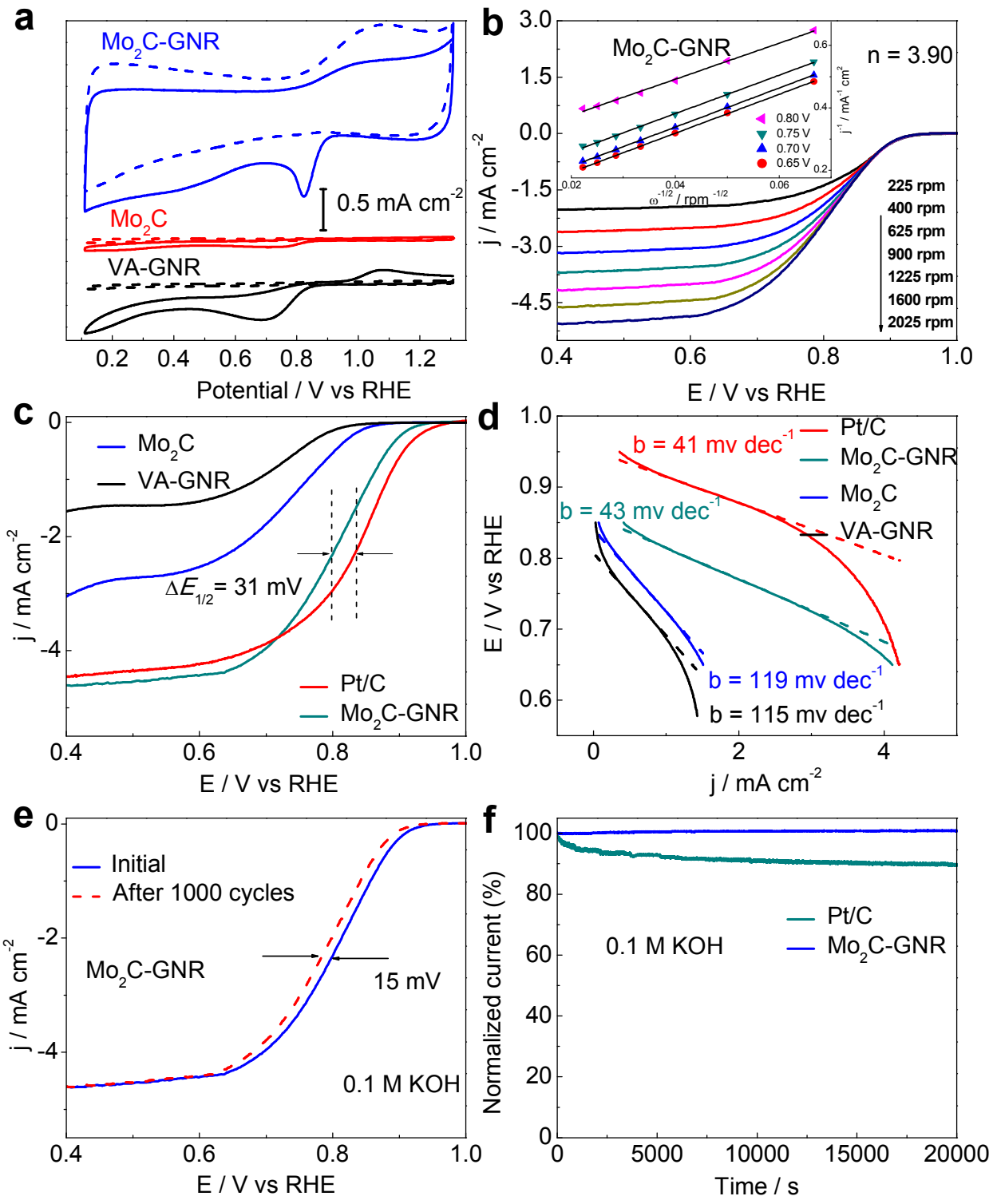

Figure 3. (a) CVs of Mo_2C-GNR, Mo_2C and VA-GNR in O_2-saturated (solid lines) and Ar-saturated (dashed lines) 0.1 M KOH electrolyte solutions at a scan rate of 5 mV s^{-1}. (b) RDE

voltammogram of Mo_2C-GNR in O_2-saturated 0.1 M KOH with a scan rate of 5 mV s^{-1} at different RDE rotation rates (rpm). (c) RDE voltammogram of Mo_2C, VA-GNR, Mo_2C-GNR and Pt/C in O_2-saturated 0.1 M KOH with a sweep rate of 5 mV s^{-1} at 1600 rpm, (d) the corresponding Tafel slopes. (e) Endurance test of the Mo_2C-GNR catalyst for 1000 cycles in O_2-saturated 0.1 M KOH. (f) Chronoamperometric responses (percentage of current retained *vs* operation time) of Mo_2C-GNR hybrid and Pt/C on carbon glass electrodes kept at 0.70 V *vs* RHE in O_2-saturated 0.1 M KOH electrolytes.

To measure the electrocatalytic activity of Mo_2C-GNR hybrid toward ORR, the as-prepared electrodes are first loaded onto glassy carbon electrodes for cyclic voltammetry (CV) in O_2-saturated and Ar-saturated 0.1 M KOH (see Supplementary Information for experimental details). The Mo_2C-GNR catalyst exhibits a pronounced active ORR activity, displaying a much more positive onset potential (~ 0.93 V *vs* RHE) and peak potential (~ 0.83 V *vs* RHE), and a higher peak current density (2.01 mA cm^{-2}) than those of Mo_2C (~ 0.84 V, 0.73 V and 0.085 mA cm^{-2}, respectively) (Figure 3a, Table S2). VA-GNR alone without any Mo_2C shows some ORR catalytic activity, but the onset potential (0.82 V) and peak potential (0.68 V) are more negative than the hybrid materials. Note that the onset potential for Pt/C catalyst (20 wt% Pt on Vulcan XC-72) is located at 0.96 V *vs* RHE, only ~ 30 mV more positive than that of the Mo_2C-GNR hybrid (Figure S14, Table S2). This suggests that Mo_2C in the Mo_2C-GNR hybrid enhances the ORR catalytic activity to approach that of Pt/C in 0.1 M KOH. The rotating-disk electrode (RDE)

measurements were employed to reveal the ORR kinetics of the Mo_2C-GNR hybrid in 0.1 M KOH (Figure 3b). The Koutecky-Levich plots are linear; the fitting lines are almost parallel, which suggests first-order reaction kinetics toward the concentration of dissolved oxygen and similar electron transfer number (n) for ORR at different potentials (Figure 3b inset). The n calculated from the the slopes of the Koutecky-Levich plots is 3.90 at 0.65-0.80 V, suggesting that the Mo_2C-GNR hybrid favors a 4 e^- oxygen reduction process, similar to a high-quality commercial Pt/C ORR catalyst measured in the same 0.1 M KOH electrolyte (n = 4.0 for Pt/C, see Supporting Information, Figure S14). Consistent results were obtained in rotating ring disk electrode (RRDE) voltammetric measurements. Figure S15a shows that the ring current (I_r) was negligible compared to the disk current (I_d); the H_2O_2 yield (Figure S15b) was below ~5% over the potential range From 0.2 to 0.7 V and gave an n of ~ 3.93, suggesting a one-step, four-electron oxygen reduction pathway. 20% Pt/C, as expected, shows an n value of ~ 4 from low (onset, n = 3.98) to high overpotential (steady-state, n = 3.98) as it generally proceeds by an efficient four-electron ORR mechanism (Figure S15c,d). On the other hand, in acidic media (0.5 M H_2SO_4), the Mo_2C-GNR possesses an onset potential (0.77 V *vs* RHE) and half-wave potential ($E_{1/2}$) (0.60 V *vs* RHE) similar to that of Pt/C (0.82 V *vs* RHE and 0.66 V *vs* RHE, respectively, Figure S16). Figure 3c reveals the linear sweep voltammograms (LSV) of the Mo_2C, VA-GNR, Mo_2C-GNR and Pt/C in O_2-saturated 0.1 M KOH solution, Mo_2C and VA-GNR exhibit poor electrocatalytic activity toward ORR in alkaline solution, while Mo_2C-GNR represents high electrocatalytic activity with a more positive onset potential. The $E_{1/2}$ of Mo_2C-GNR at 1600 rpm

is 0.80 V, similar to that of Pt/C at 0.83 V as seen in Figure S14, and more positive than that of Mo_2C at 0.74 V shown in Figure 3c. The excellent ORR activity of the Mo_2C-GNR hybrid catalyst is also indicated from the much smaller Tafel slope of 43 mV dec^{-1} at low overpotential (Figure 3d) than that measured with Mo_2C (115 mV dec^{-1}) in 0.1 M KOH, further confirming that the Mo_2C-GNR hybrid is an efficient electrochemical catalyst for ORR.

In addition, the ORR performances of Mo_2C based hybrids can be tailored *via* varying the atomic H treated time. The Mo_2C-GNR hybrid prepared with atomic H treatment for 3 h presents a lower ORR activity, as evidenced in Figure S17a, where the $E_{1/2}$, onset potential and n are 0.73 V, 0.86 V and 3.27 at 1600 rpm, respectively. The n of Mo_2C-GNR grown for 9 h and derived from the Koutecky-Levich plot, drops to 2.64, indicating a more favorable 2e reduction of O_2 toward HO_2^- (Figure S17b). The enhanced catalytic performance with atomic H treatment process for 6 h is thought to be due to the increased crystalline structure and the improved contact between Mo_2C NCs and graphene, producing a strong synergistic interaction. Due to the high thermal and chemical stability of Mo_2C-GNR hybrid obtained at high temperature, its ORR durability is high. As shown in Figure 3e, further extension of the stability test to 1000 cycles in 0.1 M KOH shows a small additional shift of the $E_{1/2}$ by 15 mV for Mo_2C-GNR. Moreover, the Mo_2C-GNR exhibits no attenuation after 20000 s in 0.1 M KOH solution, at which time 100.01 % of the relative current persists; whereas Pt/C loses nearly 12 % of its initial activity (Figure 3f), further confirming that the Mo_2C-GNR hybrid has better stability than Pt/C.

In contrast to the traditional metal carbide and other nanostructure electrocatalysts, which

are active under either acidic or basic conditions,[39] the Mo_2C-GNR catalyst prepared by HF-CVD demonstrates favorable HER activity over a wide range of pH values. The electrocatalytic activities of the Mo_2C-GNR toward HER were determined in both acidic (0.5 M H_2SO_4) and alkaline (0.1 M KOH) aqueous solutions with VA-GNR and commercial Pt for comparison (Figure 4a-c**)**. The onset overpotentials of Pt are 5 and 6 mV with Tafel slopes of 30 and 29 mV dec^{-1} in acidic and alkaline solution, respectively. For Mo_2C-GNR, the onset potentials are 39 and 53 mV, while the Tafel slopes are 65 and 54 mV dec^{-1} in acidic and alkaline solution, respectively. The HER process occurs through a Volmer-Heyrovsky mechanism, in which a fast discharge of a proton is followed by rate-limiting electrochemical recombination with an additional proton.[40] To achieve a 10 mA cm^{-2} HER current density, the Mo_2C-GNR requires overpotentials (η_{10}) of ~152 and ~121 mV in acidic and alkaline solution, respectively, which are much smaller values than those of Mo_2C, ~275 and ~266 mV, respectively (Table S3). The HER efficiency shows a maxima when the Mo_2C-GNR hybrid treated for 6 h, which is confirmed by the cathodic polarization curves and corresponding Tafel plots (Supporting Information, Figure S18). The Mo_2C-GNR hybrid electrode presents onset overpotential which is significant lower than those reported for nanoscale Mo_2C (Supporting Information, Table S3). At an overpotential of 300 mV, the maximum kinetic current density normalized to the geometric area can reach up to 106 mA cm^{-2}, which is higher than that seen in Mo_2C grown without GNR support. The corresponding Tafel slopes of the Mo_2C-GNR hybrids with various atomic H treated time are in the range of 65 to 93 mV dec^{-1} (Figure S18). Compared with CNT-GR

supported Mo_2C/CNT-GR composites,[5] Mo_2C-NCNTs[41] and other Mo-based catalysts recently reported (Supporting Information, Table S4), the Mo_2C-GNR hybrids deliver higher kinetic current densities and more positive onset overpotentials. The improved HER performances of Mo_2C-GNR are mainly ascribed to the high crystallinity and purity of Mo_2C NCs that facilitate the exposure of more active edge sites and provide more pathways for ion and mass transport.[42] Hence, Mo_2C-GNR with a treatment time of 6 h displays the highest HER activity with the most positive onset overpotential and smallest Tafel slope (Figure 4a-d) among the nanoscale class of Mo-based materials.

VA-GNR without anchored Mo_2C has negligible electrocatalytic activity, which indicates the the robust structure formed by Mo_2C and GNR reduces the energy input needed to activate HER. The exchange current densities (log (Current Density) at 0 V *vs* RHE) of Mo_2C-GNR and Mo_2C are 0.31 and 0.027 mA cm^{-2}, respectively, which are expected to be proportional to the catalytically active surface area. An alternative approach to estimate the effective surface area is to measure the capacitance of the double layer at the solid-liquid interface with CV. The capacitances for Mo_2C-GNR hybrid electrodes treated with atomic H under various time for 3, 6 and 9 h are 12.05, 22.34 and 6.14 mF cm^{-2}, respectively (Supporting Information, Figure S19). As seen in Figure 4e and S20, the capacitance of the Mo_2C-GNR and Mo_2C electrodes are 23.34 and 0.42 mF cm^{-2}, respectively. Accordingly, the roughness factor of Mo_2C-GNR and Mo_2C are 1060 and 19, respectively (Figure 4f**)**. The electrochemical surface area serves as an approximate guide for surface roughness within an order-of-magnitude accuracy.[43] Therefore, the large

exchange current density of the Mo_2C-GNR electrode is associated with its high surface area. Moreover, NCs synthesis is essential for improving the HER performance by increasing the number of catalytically active sites.[44] It is known that Mo_2C nanoparticles exhibit good electrocatalytic activity toward HER.[45] Thus, the size effect of the GNR-supported Mo_2C contributed significantly to its electrochemical performance. Figure S21 shows the Nyquist plots of Mo_2C-GNR, Mo_2C and VA-GNR. It is seen that although VA-GNR shows a slightly larger semicircle, the Faradaic impedance yielded by Mo_2C-GNR is also very small, indicating that Mo_2C-GNR have good electron transfer ability. In addition, integration of catalysts with carbon will enhance the electroconductivity. These verify that VA-GNR plays a significant role in improving the activity of electrocatalysts. The Mo_2C-GNR robust conjugation helps Mo_2C NCs coalesce strongly with the GNR (Figure 2e,f), providing a lower resistance path suitable for fast electron transfer and improve electrocatalytic activity for HER.

To assess the durability of the catalyst in acidic and alkaline environments, the practical operation of the catalyst was examined by electrolysis at fixed potentials over extended periods. As illustrated in Figure 5a, at overpotentials of -186 and -240 mV, the catalyst current densities remain stable at ~ 20 and 50 mA cm^{-2} for electrolysis over 30000 s. At a higher overpotential to drive high current density of ~ 100 mA cm^{-2}, a small loss in cathodic current density of < 5% is observed in the Mo_2C-GNR electrodes during the first 1 h. The catalytic current then keeps increasing with negligible degradation after 30000 s, revealing its excellent stability under HER conditions. While in alkaline media, the catalytic current first increases slightly, and then fully

stabilizes for the rest of the potentiostatic electrolysis (Figure 5b). The as-measured time-dependent curve shows a typical serrate shape, which can be attributed to the alternate processes of bubble accumulation and bubble release (insets of Figure 5a,b). This exceptional durability demonstrates promise for practical applications of the catalysts over longer periods. Furthermore, long-term potential cycling was performed by taking continuous CVs at an accelerated scanning rate of 50 mV s^{-1} for 1000 cycles in both acidic and alkaline media. The Mo_2C-GNR catalyst after 1000 cycles overlays almost exactly with the initial one with negligible loss of cathodic current (Figure 5c,d). This confirms that the Mo_2C-GNR catalyst is highly resistant to accelerated degradation in both acidic and alkaline media. The XPS spectra of Mo_2C-GNR with a 30000 s HER process show negligible change of the oxidation state, which confirms the excellent stability of the NCs under the long-term electrochemical cycling process (Supporting Information, Figure S22).

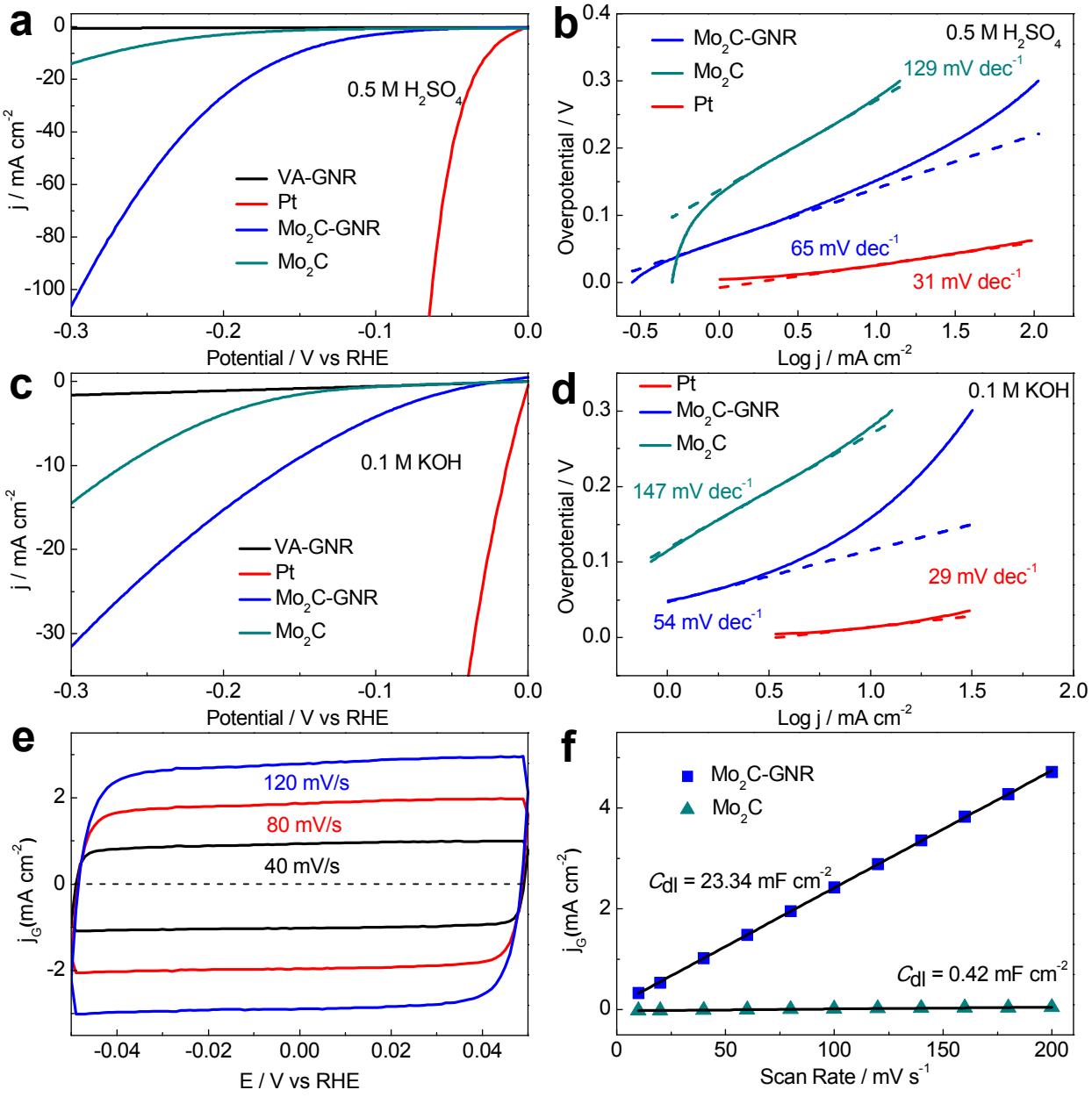

Figure 4. HER polarization curves and the corresponding Tafel plots of VA-GNR, Pt, Mo_2C-GNR and Mo_2C in (a,b) 0.5 M H_2SO_4 at pH 0 and (c,d) 0.1 M KOH at pH 13. (e) CV curves of Mo_2C-GNR and (f) corresponding differences of Mo_2C and Mo_2C-GNR in current density plotted against scan rate. The current density is measured at 0.40 and 0 V *vs* RHE for Mo_2C and Mo_2C-GNR, respectively.

Recently, group 5 disulfides (H-TaS_2 and H-NbS_2) were found to have excellent HER performance, owing to the high surface activity, which is different from molybdenum and tungsten dichalcogenides that are only edge active.[46] In Mo_2C-GNR, the GNR supports substantially increased the conductivity of the synthesized catalysts, provided high surface area to contact with electrolyte, and dispersed the Mo_2C NCs without aggregation (Figure 5e).[5] The high activity and excellent stability of the prepared Mo_2C-GNR can be related to the following properties: i) Direct growth of Mo_2C NCs on VA-GNR affords the anchored configuration of Mo_2C-GNR. This structure induces a charge-transfer from Mo_2C to carbon, which further downshifts the d-band center of Mo_2C, and thereby decreases its hydrogen binding energy.[5] This in turn favors the electrochemical desorption of H_{ads} and leads to a relatively moderate Mo-H binding strength, resulting in the enhancement of the hydrogen evolution reaction.[24] ii) The loose arrangement of Mo_2C NCs on GNR, similar to "islands" covered in graphene sheets, allows the escape of the tiny bubbles, preventing the H_2 from damaging the catalysts during the accumulation-release process, thus leading to a longer-term stability of the Mo_2C-GNR electrodes. Due to the high quality and small size of Mo_2C NCs grown on the GNR and the high electrochemical surface area, the Mo_2C-GNR hybrid also gives high ORR activity.

In addition, we find that Mo_2C can activate the "inactive" pristine graphene for HER and ORR. This is supported by our quantum-mechanical calculations, details of which are shown in the Supporting Information; the structure model for Mo_2C-graphene hybrid is shown in Figure S23. According to the Sabatier's principle, a good HER catalyst should have free energy (G) of

adsorbed H close to zero. Our calculations show that *G* for graphene is >1 eV; however, for graphene on Mo_2C, *G* decreases significantly to ~0.3 eV (Figure 5f), suggesting that the HER activity is substantially enhanced. Similarly, we find that pristine graphene does not chemically bind with OOH, a key intermediate during ORR; however, the underlying Mo_2C strengthens the binding of graphene with OOH by ~1 eV, suggesting a significantly enhanced ORR activity. The enhanced binding is associated with the relatively strong interaction (-0.1 eV C^{-1}) between graphene and Mo_2C, compared to the interaction between graphene and typical metals such as Cu, Ni, Co and Fe, at ~ -tens of meV. The strong interaction can modify the π electrons of C, making graphene more reactive.[47] In general, the 3D assembled architecture of 1D Mo_2C combined with 2D graphene sheets provides a non-precious metal catalyst for highly efficient electrocatalytic oxygen reduction and hydrogen evolution reactions.

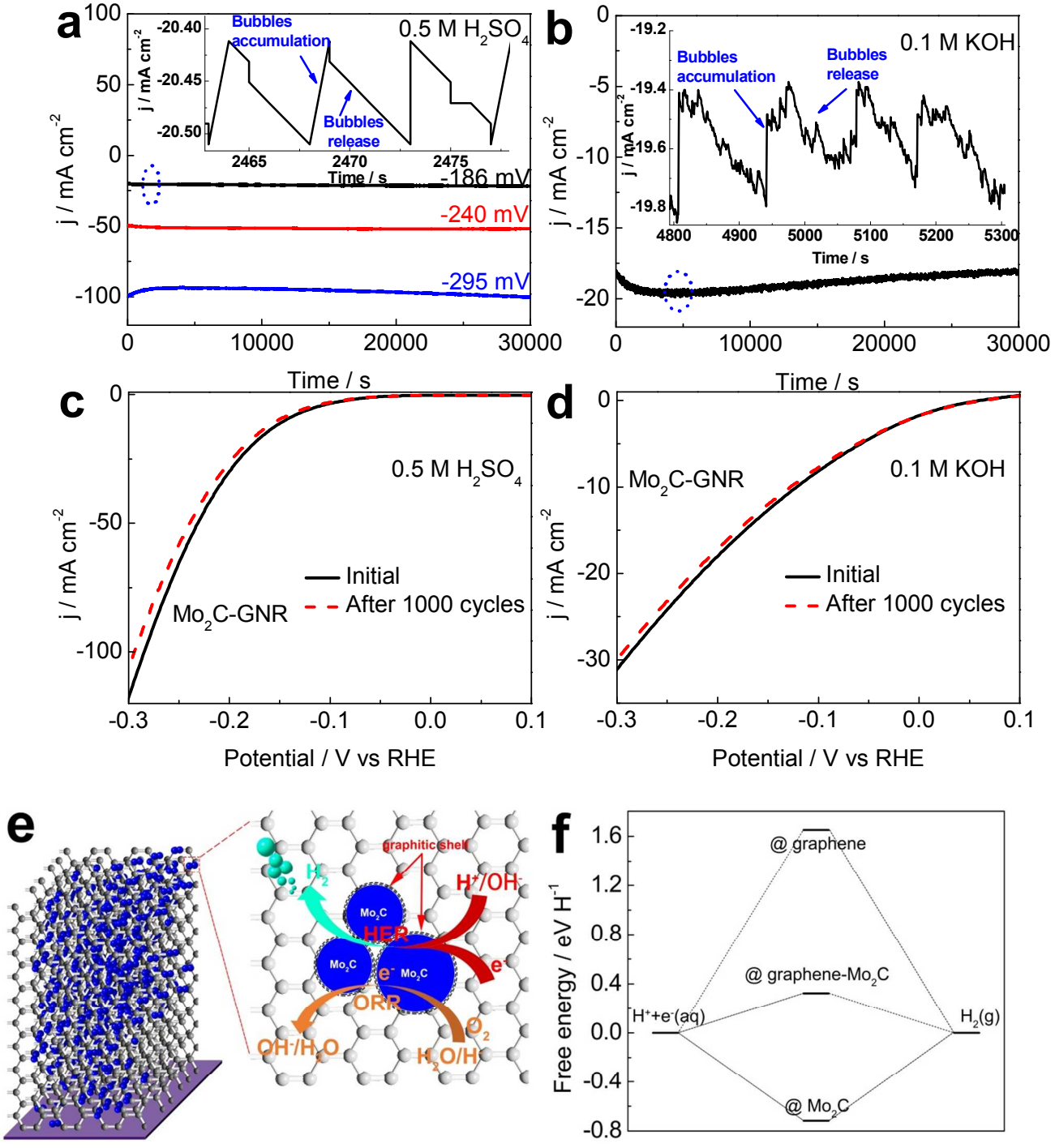

Figure 5. (a,b) Time dependence of cathodic current density during electrolysis over 30000 s in acidic and alkaline medium, respectively. Insets: enlargement of the area denoted by the dashed circle. (c,d) The first and 1000th polarization cycles for Mo_2C-GNR in acidic and alkaline media,

respectively. (e) Mechanism diagram of catalytic reaction for Mo_2C-GNR. (f) Free energy evolution of H, with respect to the standard hydrogen electrode (SHE), during HER catalyzed by various materials.

Conclusions

A precious-metal-free bifunctional electrocatalyst containing Mo_2C NCs with sufficiently small particle size (avg. 7.5 nm) on the VA-GNR is successfully synthesized using atomic H treatment. The growth mechanism of Mo_2C NCs through the direct carbonization of metallic Mo with atomic H treatment is discussed. The Mo_2C-GNR gives higher electrochemical surface area and ORR activity with a high peak current density of 2.01 mA cm^{-2} and a more positive onset potential of 0.93 V *vs* RHE in alkaline solution. The Mo_2C-GNR also exhibits efficient and durable HER activity in both acidic and alkaline media. The obtained η_{10}, onset potential, and Tafel slope values of Mo_2C-GNR hybrid are 152 mV, 39 mV, and 65 mV dec^{-1} in acid solution, and 121 mV, 53 mV, and 54 mV dec^{-1} in alkaline solution, respectively. This study introduces the potential of Mo_2C grown on the VA-GNR using atomic H treatment as a bifunctional electrocatalyst in ORR and HER.

Experimental Section

Synthesis of VA-GNR Through VA-CNTs Carpets. The VA-CNTs were synthesized as previously reported using a one-wire HF-CVD with Catalyst (1 nm Fe and 10 nm Al_2O_3).[48]

While, the VA-GNR, Mo_2C-GNR and Mo_2C were synthesized by four-wires HF-CVD. The VA-CNTs carpets were loaded into the CVD furnace chamber ~ 3-6 mm below the hot filament. An atomic H treatment was carried out using a mixture of H_2 (140 sccm), H_2O (15 sccm) and CH_4 (0.1 sccm) at 25 Torr at 850 °C for 0.5 h. The hot filament power was kept at 65 W. The VA-GNR formed a structure resembling a teepee, while the vertical integrity was still preserved.[31]

Mo_2C NCs Synthesis. In a typical synthesis, a layer of metallic Mo (~ 75 nm) was deposited on VA-GNR with a sputter deposition system. The VA-GNR with molybdenum were loaded into the CVD furnace chamber ~ 3-6 mm below the hot filament. The hot filament is the same as used to grow VA-GNR with four tungsten wires. Typically, atomic H treatment was carried out using a mixture of H_2 (140 sccm), H_2O (15 sccm) and CH_4 (0.5 sccm) at 25 Torr for 1 to 9 h. The temperature was fixed at 850 °C. The hot filament power was kept at 75 W. After treatment, the Mo_2C-GNR detached from the Si wafer simply by peeling off from the Si substrate using a blade. Alternatively, Mo_2C was also directly grown on a bare Si wafer in order to compare the difference resulting Mo_2C crystallinity and electrocatalytic performance. The catalyst with Mo_2C grown on the VA-GNR is denoted as Mo_2C-GNR, and on bare Si wafer as Mo_2C.

Characterization of the Templates and Catalysts. A Bruker D_8 Advance diffractometer (DMAX 2500) operating with a Cu Kα energy source at 40 kV and 40 mA was used to crystallographically characterize the materials. SEM and corresponding energy-dispersion X-ray spectroscopy (EDS) measurements were performed using an FEI Quanta 400 high-resolution

field emission scanning electron microscope in high-vacuum mode. XPS was conducted on a PHI Quantera SXM scanning X-ray microscope. An Al anode at 25 W was used as an X-ray source with a pass-energy of 26.00 eV, 45 take off angle, and a 100 μm beam size. TGA was performed in a Mettler-Toledo TGA-DSC1 Star system in air flow (100 mL min^{-1}). The BET surface area was measured on a Quantachrome autosorb-3b BET surface analyzer. A field-emission TEM (JEOL 2010F) with an imaging filter (Gatan GIF) was used at 200 kV to characterize the morphology and the particle size distribution of the synthesized products. The Mo content in the catalysts was obtained by ICP-MS analysis on 7700x equipment (Agilent).

Electrode Preparation and Electrochemical Characterization and HER. Taking the Mo_2C-GNR electrode as an example, the catalyst was ultrasonically dispersed in distilled water (Milli-Q) containing 0.5 wt% Nafion. An aqueous dispersion of the catalyst (40 μL, 1.0 mg mL^{-1}) was then transferred onto the glassy carbon electrode (GCE) serving as a working electrode. A Pt foil (SPI Supplies, West Chester, PA) as the counter electrode and a saturated calomel electrode (SCE) as the reference electrode. All potentials were referenced to a RHE by adding a value of (0.2415 + 0.059 × pH) V. All potentials were referenced to a RHE by adding a value of (0.2415 + 0.059 × pH) V. Prior to all measurements, the electrochemical cell was purged with H_2 bubbles for 30 min.

ORR. Electrochemical measurements were carried out as previously described.[49] An aqueous dispersion of the catalyst (40 μL, 1.0 mg mL^{-1}) was then transferred onto the glassy carbon rotating disk electrode (RDE, 0.196 cm^2, Pine Research Instrumentation, Durham, NC) or Pt

(RRDE, ring area = 0.1866 cm^2) serving as a working electrode. Hg/HgO (0.1 M KOH) (MMO, 0.098 V *vs* SHE) was used as the reference electrode. All potentials were referenced to a RHE by adding a value of (0.098 + 0.059 × pH) V.

DFT Calculations. Density functional theory (DFT) calculations were performed by using the Vienna *Ab-initio* Simulation Package (VASP)[50] with projector augmented wave (PAW) pseudopotentials,[51] and Perdew-Burke-Ernzerhof (PBE) exchange-correlation functional[52] including van der Waals corrections (DFT-D3).[53] The plane-wave cut-off energy is 400 eV, with 7x7x1 Monkhorst-Pack sampled k-points.[54] All structures are fully relaxed until the final force on each atom becomes less than 0.01 eV $Å^{-1}$. The structure model for Mo_2C-graphene hybrid is shown in **Figure S23**, with lattice mismatch less than 2%.

Acknowledgments

The authors acknowledge Y. Yang, H. Fei, R. Ye, G. Ruan, Q. Zhong, C. Gao, L. Li, N. D. Kim and J. Lin at Rice University for helpful discussions, and the National Natural Science Foundation of China (21603129), the Air Force Office of Scientific Research (FA9550-09-1-0581), and the AFOSR MURI program (FA9550-12-1-0035) for partial support of this research. The authors would also like to acknowledge Dr. Junjie Zhang from Scientific Instrument Center at Shanxi University for her help with ICP-MS measurement. Y. L. acknowledges the support from Resnick Prize Postdoctoral Fellowship at Caltech. The computations were performed on National Energy Research Scientific Computing Center, a DOE Office of Science User Facility supported by the

Office of Science of the U.S. Department of Energy under Contract No. DE-AC02-05CH11231, and Extreme Science and Engineering Discovery Environment, which is supported by National Science Foundation grant number ACI-1053575.

Supporting Information TEM, SEM, digital images, Raman, XPS, EDS, XRD, HAADF and CV spectra, plus additional calculations, tables and data can be accessed free of charge *via* the Internet at http://pubs.acs.org.

References

1. Kita, H.; Ye, S.; Gao, Y. Mass Transfer Effect in Hydrogen Evolution Reaction on Pt Single-Crystal Electrodes in Acid Solution. *J. Electroanal. Chem.* **1992**, *334*, 351-357.

2. Fournier, J.; Wrona, P. K.; Lasia, A.; Lacasse, R.; Lalancette, J. M.; Menard, H.; Brossard, L. Catalytic Influence of Commercial Ru, Rh, Pt, and Pd (~ 0, 1 Atomic Percent) Intercalated in Graphite on the Hydrogen Evolution Reaction. *J. Electrochem. Soc.* **1992**, *139*, 2372-2378.

3. Yang, T.-H.; Pyun, S.-I. An Investigation of the Hydrogen Absorption Reaction Into, and the Hydrogen Evolution Reaction From, a Pd Foil Electrode. *J. Electroanal. Chem.* **1996**, *414*, 127-133.

4. Hunt, S. T.; Nimmanwudipong, T.; Román‐Leshkov, Y. Engineering Non‐Sintered, Metal‐Terminated Tungsten Carbide Nanoparticles for Catalysis. *Angew. Chem. Int. Ed.* **2014**, *53*, 5131-5136.

5. Youn, D. H.; Han, S.; Kim, J. Y.; Kim, J. Y.; Park, H.; Choi, S. H.; Lee, J. S. Highly Active and Stable Hydrogen Evolution Electrocatalysts Based on Molybdenum Compounds on Carbon Nanotube–Graphene Hybrid Support. *ACS Nano* **2014**, *8*, 5164-5173.

6. Liao, L.; Wang, S.; Xiao, J.; Bian, X.; Zhang, Y.; Scanlon, M. D.; Hu, X.; Tang, Y.; Liu, B.; Girault, H. H. A Nanoporous Molybdenum Carbide Nanowire as an Electrocatalyst for Hydrogen Evolution Reaction. *Energy Environ. Sci.* **2014**, *7*, 387-392.

7. Ma, F.-X.; Wu, H. B.; Xia, B. Y.; Xu, C.-Y.; Lou, X. W. Hierarchical β-Mo_2C Nanotubes Organized by Ultrathin Nanosheets as a Highly Efficient Electrocatalyst for Hydrogen Production. *Angew. Chem. Int. Ed.* **2015**, *54*, 15395-15399.

8. Xiong, K.; Li, L.; Zhang, L.; Ding, W.; Peng, L.; Wang, Y.; Chen, S.; Tan, S.; Wei, Z. Ni-Doped Mo_2C Nanowires Supported on Ni Foam as a Binder-Free Electrode for Enhancing the Hydrogen Evolution Performance. *J. Mater. Chem. A* **2015**, *3*, 1863-1867.

9. Ma, L.; Ting, L. R. L.; Molinari, V.; Giordano, C.; Yeo, B. S. Efficient Hydrogen Evolution Reaction Catalyzed by Molybdenum Carbide and Molybdenum Nitride Nanocatalysts Synthesized *via* the Urea Glass Route. *J. Mater. Chem. A* **2015**, *3*, 8361-8368.

10. Sljukic, B.; Vujkovic, M.; Amaral, L.; Santos, D. M. F.; Rocha, R. P.; Sequeira, C. A. C.; Figueiredo, J. L. Carbon-Supported Mo_2C Electrocatalysts for Hydrogen Evolution Reaction. *J. Mater. Chem. A* **2015**, *3*, 15505-15512.

11. Wang, S.; Wang, J.; Zhu, M.; Bao, X.; Xiao, B.; Su, D.; Li, H.; Wang, Y. Molybdenum-Carbide-Modified Nitrogen-Doped Carbon Vesicle Encapsulating Nickel

Nanoparticles: A Highly Efficient, Low-Cost Catalyst for Hydrogen Evolution Reaction. *J. Am. Chem. Soc.* **2015**, *137*, 15753–15759.

12. He, C.; Tao, J. Synthesis of Nanostructured Clean Surface Molybdenum Carbides on Graphene Sheets as Efficient and Stable Hydrogen Evolution Reaction Catalysts. *Chem. Commun.* **2015**, *51*, 8323-8325.

13. Pan, L. F.; Li, Y. H.; Yang, S.; Liu, P. F.; Yu, M. Q.; Yang, H. G. Molybdenum Carbide Stabilized on Graphene with High Electrocatalytic Activity for Hydrogen Evolution Reaction. *Chem. Commun.* **2014**, *50*, 13135-13137.

14. Zhang, K.; Zhao, Y.; Zhang, S.; Yu, H.; Chen, Y.; Gao, P.; Zhu, C. MoS_2 Nanosheet/Mo_2C-Embedded N-Doped Carbon Nanotubes: Synthesis and Electrocatalytic Hydrogen Evolution Performance. *J. Mater. Chem. A* **2014**, *2*, 18715-18719.

15. Liu, Y.; Yu, G.; Li, G.-D.; Sun, Y.; Asefa, T.; Chen, W.; Zou, X. Coupling Mo_2C with Nitrogen-Rich Nanocarbon Leads to Efficient Hydrogen-Evolution Electrocatalytic Sites. *Angew. Chem. Int. Ed.* **2015**, *54*, 10752-10757.

16. Cui, W.; Cheng, N.; Liu, Q.; Ge, C.; Asiri, A. M.; Sun, X. Mo_2C Nanoparticles Decorated Graphitic Carbon Sheets: Biopolymer-Derived Solid-State Synthesis and Application as an Efficient Electrocatalyst for Hydrogen Generation. *ACS Catal.* **2014**, *4*, 2658-2661.

17. Ma, R.; Zhou, Y.; Chen, Y.; Li, P.; Liu, Q.; Wang, J. Ultrafine Molybdenum Carbide Nanoparticles Composited with Carbon as a Highly Active Hydrogen‐Evolution Electrocatalyst. *Angew. Chem. Int. Ed.* **2015**, *54*, 14723-14727.

18. Rosa, C. J. Carbon Diffusion in Mo_2C as Determined from Carburization of Mo. *Metall. Trans. A* **1983**, *14*, 199-202.

19. Oyama, S. T. Preparation and Catalytic Properties of Transition Metal Carbides and Nitrides. *Catal. Today* **1992**, *15*, 179-200.

20. Kolel-Veetil, M. K.; Qadri, S. B.; Osofsky, M.; Keller, T. M. Formation of a Superconducting Mixture of β-Mo_2C Nanoparticles and Carbon Nanotubes in an Amorphous Matrix of Molybdenum Compounds by the Pyrolysis of a Molybdenum Derivative of a Carboranylenesiloxane. *Chem. Mater.* **2005**, *17*, 6101-6107.

21. Wang, H.-M.; Wang, X.-H.; Zhang, M.-H.; Du, X.-Y.; Li, W.; Tao, K.-Y. Synthesis of Bulk and Supported Molybdenum Carbide by a Single-Step Thermal Carburization Method. *Chem. Mat.* **2007**, *19*, 1801-1807.

22. Wolden, C. A.; Pickerell, A.; Gawai, T.; Parks, S.; Hensley, J.; Way, J. D. Synthesis of β-Mo_2C Thin Films. *ACS. Appl. Mater. Interfaces* **2011**, *3*, 517-521.

23. Pol, V. G.; Pol, S. V.; Gedanken, A. One‐Step Synthesis and Characterization of SiC, Mo_2C, and WC Nanostructures. *Eur. J. Inorg. Chem.* **2009**, *2009*, 709-715.

24. Chen, W. F.; Wang, C. H.; Sasaki, K.; Marinkovic, N.; Xu, W.; Muckerman, J. T.; Zhu, Y.; Adzic, R. R. Highly Active and Durable Nanostructured Molybdenum Carbide Electrocatalysts for Hydrogen Production. *Energy Environ. Sci.* **2013**, *6*, 943-951.

25. Halim, J.; Kota, S.; Lukatskaya, M. R.; Naguib, M.; Zhao, M. Q.; Moon, E. J.; Pitock, J.; Nanda, J.; May, S. J.; Gogotsi, Y. Synthesis and Characterization of 2D Molybdenum Carbide

(MXene). *Adv. Funct. Mater.* **2016**, *26*, 3118–3127.

26. Mohapatra, D. R.; Lee, H.-J.; Sahoo, S.; Lee, W.-S. A Novel Structure of Tungsten Carbide Nanowalls Grown on Nanocrystalline Diamond Film. *CrystEngComm* **2012**, *14*, 2222-2228.

27. Fan, X.; Peng, Z.; Ye, R.; Zhou, H.; Guo, X. M_3C (M: Fe, Co, Ni) Nanocrystals Encased in Graphene Nanoribbons: An Active and Stable Bifunctional Electrocatalyst for Oxygen Reduction and Hydrogen Evolution Reactions. *ACS Nano* **2015**, *9*, 7407-7418.

28. Sundaresan, S. G.; Davydov, A. V.; Vaudin, M. D.; Levin, I.; Maslar, J. E.; Tian, Y.-L.; Rao, M. V. Growth of Silicon Carbide Nanowires by a Microwave Heating-Assisted Physical Vapor Transport Process Using Group VIII Metal Catalysts. *Chem. Mater.* **2007**, *19*, 5531-5537.

29. Pang, M.; Li, C.; Ding, L.; Zhang, J.; Su, D.; Li, W.; Liang, C. Microwave-Assisted Preparation of Mo_2C/CNTs Nanocomposites as Efficient Electrocatalyst Supports for Oxygen Reduction Reaction. *Ind. Eng. Chem. Res.* **2010**, *49*, 4169-4174.

30. Liao, L.; Bian, X.; Xiao, J.; Liu, B.; Scanlon, M. D.; Girault, H. H. Nanoporous Molybdenum Carbide Wires as an Active Electrocatalyst towards the Oxygen Reduction Reaction. *Phys. Chem. Chem. Phys.* **2014**, *16*, 10088-10094.

31. Fan, X.; Peng, Z.; Yang, Y.; Zhou, H.; Guo, X. Atomic H-induced Cutting and Unzipping of Single-Walled Carbon Nanotube Carpets with Teepee Structure and their Enhanced Supercapacitor Performance. *J. Mater. Chem. A* **2015**, *3*, 10077-10084.

32. Zou, Y.; May, P.; Viera, S.; Fox, N. Field Emission from Diamond-Coated Multiwalled Carbon Nanotube “Teepee” Structures. *J. Appl. Phys.* **2012**, *112*, 044903.

33. Mestl, G.; Ruiz, P.; Delmon, B.; Knozinger, H. Oxygen-Exchange Properties of MoO_3: an *in situ* Raman Spectroscopy Study. *J. Phys. Chem.* **1994**, *98*, 11269-11275.

34. Luo, Y.; Wang, Z.; Fu, Y.; Jin, C.; Wei, Q.; Yang, R. *In situ* Preparation of Hollow Mo_2C-C Hybrid Microspheres as Bifunctional Electrocatalysts for Oxygen Reduction and Evolution Reactions. *J. Mater. Chem. A* **2016**, *4*, 12583-12590.

35. Reina, A.; Jia, X.; Ho, J.; Nezich, D.; Son, H.; Bulovic, V.; Dresselhaus, M. S.; Kong, J. Large Area, Few-Layer Graphene Films on Arbitrary Substrates by Chemical Vapor Deposition. *Nano Lett.* **2009**, *9*, 30-35.

36 Zhang, Y.; Jiang, W.-J.; Guo, L.; Zhang, X.; Hu, J.-S.; Wei, Z.; Wan, L.-J. Confining Iron Carbide Nanocrystals inside CN_x@CNT toward an Efficient Electrocatalyst for Oxygen Reduction Reaction. *ACS. Appl. Mater. Interfaces* **2015**, *7*, 11508-11515.

37 Scanlon, D. O.; Watson, G. W.; Payne, D. J.; Atkinson, G. R.; Egdell, R. G.; Law, D. S. L. Theoretical and Experimental Study of the Electronic Structures of MoO_3 and MoO_2. *J. Phys. Chem. C* **2010**, *114*, 4636-4645.

38 Liang, C.; Ying, P.; Li, C. Nanostructured β-Mo_2C Prepared by Carbothermal Hydrogen Reduction on Ultrahigh Surface Area Carbon Material. *Chem. Mater.* **2002**, *14*, 3148-3151.

39. Shen, X.; Pantelides, S. T. Atomic-Scale Mechanism of Efficient Hydrogen Evolution at SiC Nanocrystal Electrodes. *J. Phy. Chem. Lett.* **2012**, *4*, 100-104.

40. Li, Y.; Wang, H.; Xie, L.; Liang, Y.; Hong, G.; Dai, H. MoS_2 Nanoparticles Grown on Graphene: An Advanced Catalyst for the Hydrogen Evolution Reaction. *J. Am. Chem. Soc.* **2011**,

133, 7296-7299.

41. Zhang, K.; Zhao, Y.; Fu, D.; Chen, Y. Molybdenum Carbide Nanocrystal Embedded N-Doped Carbon Nanotubes as Electrocatalysts for Hydrogen Generation. *J. Mater. Chem. A* **2015**, *3*, 5783-5788.

42. Shen, M.; Ruan, C.; Chen, Y.; Jiang, C.; Ai, K.; Lu, L. Covalent Entrapment of Cobalt–Iron Sulfides in N-Doped Mesoporous Carbon: Extraordinary Bifunctional Electrocatalysts for Oxygen Reduction and Evolution Reactions. *ACS. Appl. Mater. Interfaces* **2014**, *7*, 1207-1218.

43. McCrory, C. C. L.; Jung, S.; Peters, J. C.; Jaramillo, T. F. Benchmarking Heterogeneous Electrocatalysts for the Oxygen Evolution Reaction. *J. Am. Chem. Soc.* **2013**, *135*, 16977-16987.

44. Wang, H.; Zhang, Q.; Yao, H.; Liang, Z.; Lee, H.-W.; Hsu, P.-C.; Zheng, G.; Cui, Y. High Electrochemical Selectivity of Edge *versus* Terrace Sites in Two-Dimensional Layered MoS_2 Materials. *Nano Lett.* **2014**, *14*, 7138–7144.

45. Wan, C.; Regmi, Y. N.; Leonard, B. M. Multiple Phases of Molybdenum Carbide as Electrocatalysts for the Hydrogen Evolution Reaction. *Angew. Chem.* **2014**, *126*, 6525–6528.

46. Liu, Y.; Wu, J.; Hackenberg, K. P.; Zhang, J.; Wang, Y. M.; Yang, Y.; Keyshar, K.; Gu, J.; Ogitsu, T.; Vajtai, R. Self-Optimizing Layered Hydrogen Evolution Catalyst with High Basal-Plane Activity. *arXiv:* **2016**, *1608.05755.*

47. Liu, Y.; Wang, Y. M.; Yakobson, B. I.; Wood, B. C. Assessing Carbon-Based Anodes for Lithium-Ion Batteries: A Universal Description of Charge-Transfer Binding. *Phys. Rev. Lett.* **2014**, *113*, 028304.

48. Pint, C. L.; Xu, Y.-Q.; Moghazy, S.; Cherukuri, T.; Alvarez, N. T.; Haroz, E. H.; Mahzooni, S.; Doorn, S. K.; Kono, J.; Pasquali, M.; Hauge, R. H. Dry Contact Transfer Printing of Aligned Carbon Nanotube Patterns and Characterization of Their Optical Properties for Diameter Distribution and Alignment. *ACS Nano* **2010**, *4*, 1131-1145.

49. Xiao, J. W.; Kuang, Q.; Yang, S. H.; Xiao, F.; Wang, S.; Guo, L. Surface Structure Dependent Electrocatalytic Activity of Co_3O_4 Anchored on Graphene Sheets toward Oxygen Reduction Reaction. *Sci. Rep.* **2013**, *3*, 8.

50. Kresse, G.; Hafner, J. *Ab initio* Molecular Dynamics for Liquid Metals. *Phys. Rev. B* **1993**, *47*, 558-561.

51. Blöchl, P. E. Projector Augmented-Wave Method. *Phys. Rev. B* 1994, 50, 17953-17979.

52. Perdew, J. P.; Burke, K.; Ernzerhof, M. Generalized Gradient Approximation Made Simple. *Phys. Rev. Lett.* **1996**, *77*, 3865-3868.

53. Grimme, S.; Antony, J.; Ehrlich, S.; Krieg, H. A Consistent and Accurate *ab initio* Parametrization of Density Functional Dispersion Correction (DFT-D) for the 94 Elements H-Pu. *J. Chem. Phys.* **2010**, *132*, 154104.

54. Monkhorst, H. J.; Pack, J. D. Special Points for Brillouin-Zone Integrations. *Phys. Rev. B* **1976**, *13*, 5188-5192.

TOC graphic